



A novel approach to finding mechanical properties of nanocrystal layers

Journal:	<i>Nanoscale</i>
Manuscript ID	NR-ART-03-2019-002213
Article Type:	Paper
Date Submitted by the Author:	13-Mar-2019
Complete List of Authors:	Sinha, Mayank; Michigan State University, Mechanical Engineering Izadi, Alborz; Michigan State University, Mechanical Engineering Anthony, Rebecca; Michigan State University, Mechanical Engineering Roccabianca, Sara; Michigan State University, Mechanical Engineering



Cite this: DOI: 10.1039/xxxxxxxxxx

A novel approach to finding mechanical properties of nanocrystal layers

Mayank Sinha[‡], Alborz Izadi[‡], Rebecca Anthony^{*}, and Sara RoccabiancaReceived Date
Accepted Date

DOI: 10.1039/xxxxxxxxxx

www.rsc.org/journalname

Flexible, bendable, stretchable devices represent the future of electronics for a wide range of real-world applications. Due to the fact that these technologies deviate significantly from traditional wafer technologies there is a need to understand and engineer material systems that allow large elastic deformations present in such devices, which requires knowledge about the mechanical properties of these material systems. Here we evaluate the mechanical properties of a bilayer polydimethylsiloxane (PDMS)/silicon nanocrystal system. By observing the formation of instabilities due to finite bending deformation and applying theoretical modeling, we estimated the neo-Hookean coefficient (analogous to shear modulus at low stress/strain) of the SiNC film to be 345 ± 23 kPa. The method used here represents a novel approach to evaluating these properties and is widely applicable to many different combinations of systems of nanocrystals and elastomers.

1 Introduction

As flexible devices become more prevalent, it is increasingly important to measure and predict the mechanical properties of active device layers, including thin films^{1–3}. Nanoscale components, such as nanocrystals, can be incorporated into mechanically flexible devices^{1,4}. Silicon in its nanocrystal form has semiconducting and photoluminescence properties which make it a promising material for technologies like microelectronics^{5–7}, photonics^{7,8}, solar-photovoltaics^{9,10}, memory devices¹¹, biosensors, and light emitting devices^{12,13}, as well as other applications involving polymer matrices^{14,15}. Using silicon nanocrystals in these applications is particularly attractive considering the natural abundance and non-toxicity of silicon. In most of the aforementioned applications, silicon nanocrystals (SiNCs) are deposited on rigid substrates. Depositing a SiNC film onto stretchable or flexible substrates opens up possibilities for new device development and modifications¹⁶. While the opportunity of designing these devices is exciting, it also highlights the need for an innovative way to estimate mechanical properties for these systems.

Substantial work has been done by various groups on studying the mechanical properties of nanocrystalline materials, both in the elastic^{17,18} and plastic^{19–23} regimes. Some works also discuss the significant differences in mechanical properties of nanocrystalline material from their bulk counterparts^{17–20,22–25}.

These testing techniques, while powerful in estimating the material properties for a large variety of nanocrystalline materials, inherently require the destruction of the samples or the plastic deformation of the material. This is in conflict with the scope of this work, which is focusing on non-destructive techniques to estimate elastic behavior of thin layers of nanocrystals on deformable substrates. These combined systems limit *in-situ* measurement of the layers' mechanical properties such as elastic modulus. This necessitates finding an appropriate method to understand and predict the response of not just the nanocrystal layers during deformation, but of the whole elastomer-nanocrystal layer system. Indeed, *in-situ* evaluation of mechanical behavior is crucial for thin layers, for which interactions between the substrate and the thin film can be as important as the properties of the thin film itself. To our knowledge, such *in-situ* evaluation of the mechanical properties of SiNC layers on elastomers has not been previously reported.

Prior *in-situ* studies on nanoscale materials have employed microscopy during uniaxial tensile testing to observe deformation under applied loads^{22,23,26}. Barring the specialty equipment necessary for these experiments, a promising option that has been used in the last two decades to estimate material properties of thin films is to measure the onset of instability patterns on the surface of the thin film due to different loading conditions²⁷. This technique has the advantage of being simple, inexpensive, and non-destructive; furthermore it can be applied to any type of thin layer deposited on a deformable substrate. Because of its flexibility, this method has been employed to estimate mechanical properties of several isolated thin films^{28–30} or multi-layered

Michigan State University, East Lansing, MI, USA. Fax: 517-353-1750; Tel:517-432-7491; E-mail: ranthony@egr.msu.edu

[‡]These authors contributed equally to this work

structures^{31–34}. All of these studies focused on applying homogeneous deformations, namely uniaxial tension or compression, to the system. However, other types of non-homogeneous loading conditions, such as bending, can also lead to the formation of instabilities. In the past, several studies have focused on developing a theoretical framework to describe the onset of instabilities on the surface of rectangular blocks subject to finite bending^{35–44}. The framework developed in these works focused only on finite bending deformation for a homogeneous block. These early predictions have also been recently confirmed by experimental work^{37,39}. In the last decade, a few studies focused on predicting bifurcations during finite bending of multi-laminated structures, specifically in bilayered systems, both theoretically and experimentally^{41,42}.

A recent study on the optical and structural properties of SiNCs on polydimethylsiloxane (PDMS) demonstrated the formation of instabilities on a nanocrystal film deposited on a prestretched elastomer⁴⁵. Combining the onset of instabilities with the predictions from the theoretical modeling framework described, we evaluate the mechanical properties of the SiNC thin film deposited on an elastomeric substrate. This theoretical framework can further be applied to different combinations of nanocrystals and elastomers, for *in situ* measurement of mechanical properties of such bilayered systems.

2 Methods

Here we take a novel approach to evaluate the mechanical properties of thin films of nanocrystals on an elastomeric substrate. A PDMS-SiNC bilayer was used as a model to present the framework. First, we inertially impacted a uniform film of SiNCs on PDMS. Then, we applied a finite bending deformation to the system until instabilities formed on the surface coated with the SiNCs, noting the critical angle at which the instabilities appeared. Finally, we applied a theoretical modeling framework to describe the bilayer system. See Fig. 1 for an overview of our process.

2.1 PDMS Fabrication

To manufacture the PDMS, a Dow Corning heat-cured 184 Sylgard Elastomer PDMS kit was used with a 10:1 weight ratio of base to curing agent. This mixture was stirred vigorously until air bubbles formed, and placed under vacuum for 15 minutes to remove the trapped air. The mixture was then weighed and poured into a petri dish of 85 mm diameter and was cured for 120 minutes at 60°C by placing on a hot plate to form PDMS of thickness 2.5 mm. After curing, the PDMS was cut in rectangular sections according to our requirements and then attached to two metallic handles with Gorilla[®] Super Glue as shown in Fig.1b and d.

2.2 Plasma synthesis of SiNCs

We produced the SiNCs using a nonthermal plasma reactor as has been reported previously^{45–48}. The reactor consists of a pyrex tube through which we flow 94 sccm (standard cubic centimeters per minute) of Argon (Ar) and 16 sccm of silane (SiH₄, 5% in Ar), as well as 50 sccm of H₂ through the sidearm for surface passi-

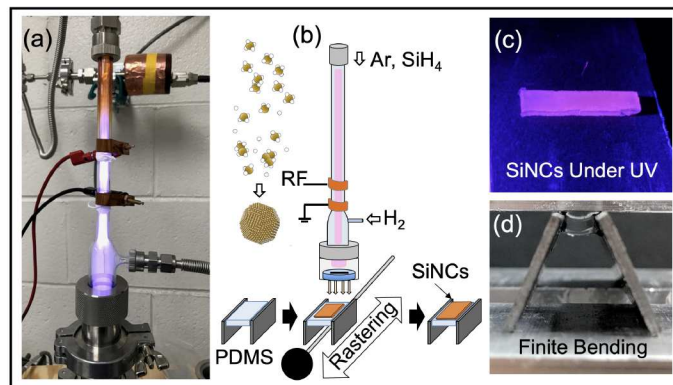


Fig. 1 Steps from plasma deposition to finite bending. SiNCs are deposited through a slit-shaped orifice onto PDMS, which is then bent to observe formation of wrinkles on the SiNC surface. (a) Photograph of plasma reactor. (b) Schematic diagram of reactor and SiNC synthesis. (c) SiNC/PDMS sample illuminated with UV light, demonstrating photoluminescence. (d) Finite bending applied with a lab-designed apparatus.

vation. Radiofrequency (RF) power at 13.56 MHz was supplied to dual ring electrodes encircling the reactor, and the pressure was kept constant at 3.85 Torr using a slit-shaped orifice. The standoff distance between the orifice and the substrate was ~ 4 mm. The downstream pressure was ~ 0.5 Torr. The nanocrystals were deposited in thin films by inertial impaction directly out of the reactor onto the substrate.^{13,49–51} One of the assets of this synthesis method is the room-temperature process and ability to directly deposit SiNCs without post-processing steps or solvents, even on temperature-sensitive substrates such as PDMS. The PDMS samples were made (as described in Sec. 2.1), attached to a pushrod, and placed under the orifice downstream of the reactor. The SiNCs were deposited by rasting the substrate back and forth beneath the orifice to achieve a uniform film of SiNCs on the PDMS. Fig.1b shows a work-flow schematic of the reactor and deposition of SiNCs on the PDMS. The rasting duration was 20 minutes with each back and forth movement lasting 3 seconds, resulting in a SiNC layer thickness of ~ 4.5 μm .

2.3 Silicon Nanocrystal Film Characterization

The thickness of the sample was measured by scanning electron microscope (SEM) imaging of a cross-section of the sample generated using a focused ion beam (FIB). Fig.2a shows an SEM image of the sample, and Fig.2b shows the FIB-generated cross section for thickness estimation. To decrease charging effects and improve the image quality of the SiNC film, a thin layer of Platinum (Pt) (~ 6 nm) was deposited via Ar plasma sputtering prior to imaging. X-ray diffraction (XRD), shown in Fig.3a, confirms the formation of crystalline nanoparticles. Transmission electron microscopy (TEM) was performed on the SiNCs using a JEOL 2200 instrument, showing individual NCs (Fig.3b). The TEM sample was prepared by tapping the TEM grid on the surface of the sam-

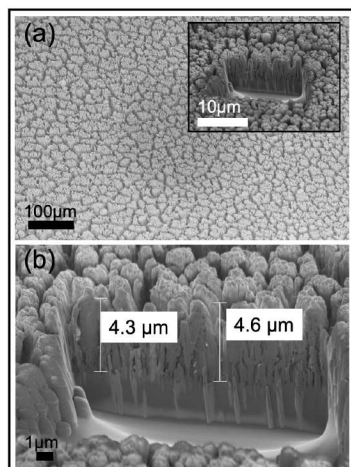


Fig. 2 SEM and FIB cross-sectioning of the SiNC layer. The thickness is estimated to be ($\sim 4.50 \mu\text{m}$). (a) SEM image showing the surface of the SiNC layer on PDMS, including the FIB-milled area (inset). (b) Higher magnification SEM image of the FIB-milled area demonstrating the thickness of the SiNC layer.

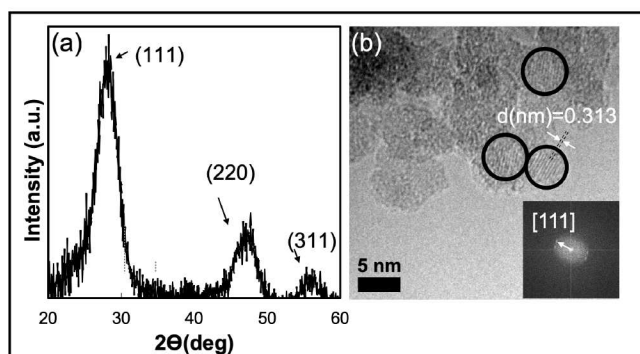


Fig. 3 (a) X-ray diffraction confirmed formation of SiNCs. XRD for SiNCs shows crystal reflections at 2θ values 28.3, 47.3 and 56.1 degrees consistent with the (111), (220), and (311) planes of silicon. (b) TEM image confirming the formation of SiNCs: black circles highlight individual SiNCs. The inset shows FFT of the correspondig SiNCs of the TEM image.

ple to collect some of the SiNCs. The size of the SiNCs was measured using TEM image analysis, giving an average SiNC diameter of $\sim 3.7 \text{ nm}$.

2.4 Uniaxial Tensile Test

We performed a standard uniaxial tensile test to evaluate the mechanical properties of the PDMS. A rectangular sample of clear PDMS was mounted on a custom built uniaxial tensile test machine and four black dots were applied on it as fiducial markers. The sample was then stretched cyclically for 5 cycles from a con-

figuration with a 10g pre-load (*i.e.*, reference configuration) until a 20% deformation was achieved. The sample was stretched between two clamps, one of which was attached to a load cell to measure the force on line with the applied deformation. The strain rate used during the tensile test was 0.1 mm/s. The force from the load cell was converted to engineering stress by calculating the average cross-section area of the sample in the reference configuration. A Hitachi KP-M2AN CCD camera was used to capture and feed the image of the fiducial markers during uniaxial stretch into LabVIEW.

2.5 Finite Bending Experiment

We created a finite bending apparatus similar to the one used previously by Roccabianca *et al.* (2010). Two important parameters are slenderness ratio ($\Lambda = l_0/h_0$) which is the ratio of width to thickness of the sample in cross section, and thickness ratio ($H = h_0^{NC}/h_0^P$) which is the ratio of thickness of the SiNC layer by that of the PDMS before finite bending (see Fig. 5a for reference). The third dimension is taken to be 8-10 times larger than l_0 to achieve a plane-strain condition on the cross section. Here (and in all following equations) the superscript 'P' refers to the PDMS and 'NC' refers to the SiNCs.

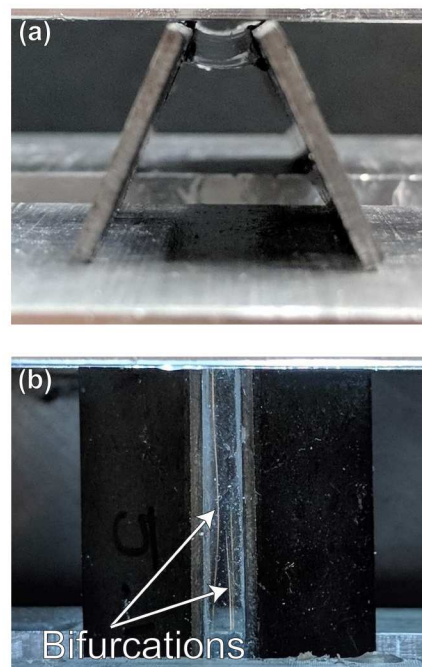


Fig. 4 PDMS sample in the finite bending apparatus. (a) Side view, showing sample (with handles) in the finite bending apparatus. (b) Top view showing formation of bifurcations.

The bilayer PDMS/SiNC system was put in the finite bending apparatus (see Fig.4) and progressively bent until the SiNC film underwent bifurcation, at which point the critical angle was recorded. Due to higher critical angles of bifurcation observed for samples with higher slenderness ratios, deformation was applied by hand instead of using the apparatus. The onset of bifurcations was detected by direct visual inspection, and the critical angle

was measured using analysis of photographs of the side view of the sample. Each measurement was performed three times to ensure accurate and reproducible readings.

2.6 Modeling bifurcations in elastic layered structures

Roccabianca *et al.* (2010), formulated a theoretical framework to study incremental bifurcations due to finite bending of an elastic incompressible multilayered block.⁴¹ This theory was developed for an N-layered system for Mooney-Rivlin type of material. The authors also performed some experiments in bilayered structures that confirmed their theoretical predictions. Here, we employ a similar theoretical modeling framework for the bilayered system to estimate the ratio of mechanical properties of SiNC thin film to that of PDMS.

2.6.1 Finite deformation

The finite bending deformation is prescribed such that the reference configuration is rectangular and described in a Cartesian coordinate system, and the deformed configuration is a sector of ring described in a cylindrical coordinate system (see Fig. 5).

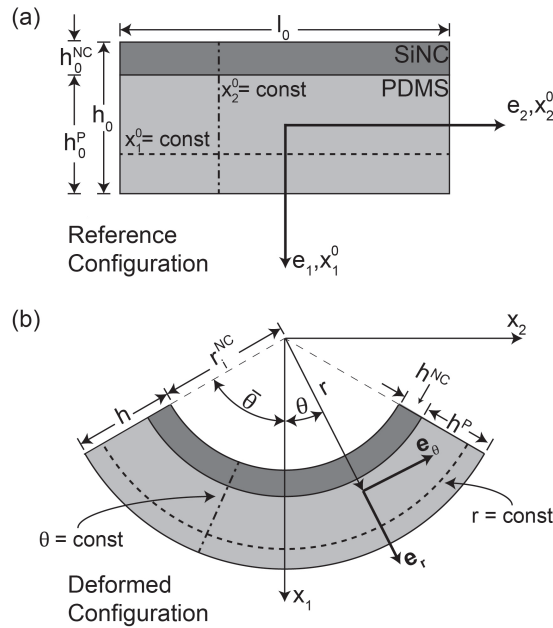


Fig. 5 Reference and deformed configurations for the PDMS-SiNC bilayer. The bilayer deforms from the Cartesian coordinate system in the reference configuration (e_1, e_2, e_3) to a cylindrical coordinate system in the deformed configuration (e_r, e_θ, e_z). Specifically, a plane at constant x_1^0 transforms to a plane at constant r (dashed line), and a plane at constant x_2^0 transforms to a circular arc at constant θ (dashed-dotted line). Since the out of plane deformation is taken to be zero, we have $x_3^0 = z$.

Briefly, the finite bending deformation can be described, within both the PDMS and the SiNC layers, by the following deformation gradient \mathbf{F} ⁴¹

$$\mathbf{F} = \frac{l_0}{2\bar{\theta}r} \mathbf{e}_r \otimes \mathbf{e}_1^0 + \frac{2\bar{\theta}r}{l_0} \mathbf{e}_\theta \otimes \mathbf{e}_2^0 + \mathbf{e}_z \otimes \mathbf{e}_3^0, \quad (1)$$

where l_0 is the overall width of the sample and $2\bar{\theta}$ is the angular deformation of the sample. We consider the volume of the

system to be conserved and the two layers to be perfectly bonded. Therefore, we can apply the interface condition $r_o^{NC} = r_i^P$, where r_o^{NC} and r_i^P are the outer radius of the SiNCs layer and the inner radius of the PDMS, respectively. This allows us to write,

$$r_o^{NC}(h_0^{NC}, h^{NC}, \alpha) = r_i^P(h_0^P, h^P, \alpha), \quad (2)$$

where h_0^m and h^m represent the thickness of each layer before and after bending ($m = NC, P$), and $\alpha = 2\bar{\theta}/l_0$. To predict all geometrical characteristics of the deformed state, we consider all the layers to be equilibrated. Briefly, we define the Cauchy stress in each layer as,

$$\mathbf{T} = -\pi\mathbf{I} + \mathbf{F} \frac{dW}{d\mathbf{C}} \mathbf{F}^T, \quad (3)$$

where $\mathbf{C} = \mathbf{F}^T \mathbf{F}$ and \mathbf{I} are the right Cauchy-Green deformation tensor and the identity tensor, respectively, and W and π are the strain energy function and the Lagrange multiplier for each layer, respectively. We have employed the neo-Hookean strain energy function to describe both layers, defined as $W = \frac{\mu_0}{2}(\text{tr}\mathbf{C} - 3)$. Note that we are defining two constitutive equations, one for the PDMS layer as a function of the material parameter μ_0^P , and one for the SiNC layer as a function of the material parameter μ_0^{NC} .

For the layers to be equilibrated, the equilibrium equation in absence of body forces is required to be satisfied within each layer. Furthermore, boundary conditions of zero traction are applied at the innermost and outermost surfaces, as well as an interface condition of perfect bonding between the two layers.

2.6.2 Bifurcation Analysis

The loss of uniqueness of the plane-strain incremental boundary value problem has been investigated for multi-layered structures in previously published work⁴¹. Here we have adapted the formulation to fit our application for a bilayered system of PDMS and SiNCs. Briefly, for each layer, we seek to solve the incremental counterpart of the equilibrium, $\text{div}(\boldsymbol{\Sigma}) = \mathbf{0}$, where $\boldsymbol{\Sigma} = \dot{\mathbf{S}}\mathbf{F}^T$ is the incremental first Piola-Kirchhoff stress tensor, and the first Piola-Kirchhoff stress and the Cauchy stress tensors are related by $\mathbf{S} = \mathbf{T}\mathbf{F}^{-T}$ for incompressible materials. Here, and in the following, we use a superimposed dot to represent incremental quantities. The linearized constitutive equation for each layer is given by

$$\boldsymbol{\Sigma} = -\dot{\pi}\mathbf{I} + \mathbb{C}\mathbf{L} \quad (4)$$

where \mathbb{C} is the fourth-order tensor of instantaneous elastic moduli and $\mathbf{L} = \text{grad } \mathbf{u}$ is the gradient of incremental displacement $\mathbf{u}(\mathbf{x})$. We consider bifurcations to be represented within each layer by an incremental displacement field in a separable-variables form, as described by Roccabianca *et al.* (2010). For incompressible isotropic elastic materials, one can write \mathbb{C} as a function of two incremental moduli, namely μ and μ^* . For neo-Hookean materials subject to finite bending in plane strain condition, the elastic moduli can be written as⁵²

$$\mu = \mu^* = \frac{\mu_0}{2} [(\alpha r)^2 + (\alpha r)^{-2}]. \quad (5)$$

Finally, the incremental boundary value problem is completed by a set of boundary and interface conditions. Specifically, zero

normal and shear incremental stresses at the innermost and outermost layer, zero incremental shear stress and incremental radial displacement at the boundary $\theta = \pm\bar{\theta}$, and continuity of incremental stresses and displacements across the interface. To calculate the angle that satisfies the bifurcation condition, θ_{cr} , we employed the compound matrix method, as described in a previously published study⁴².

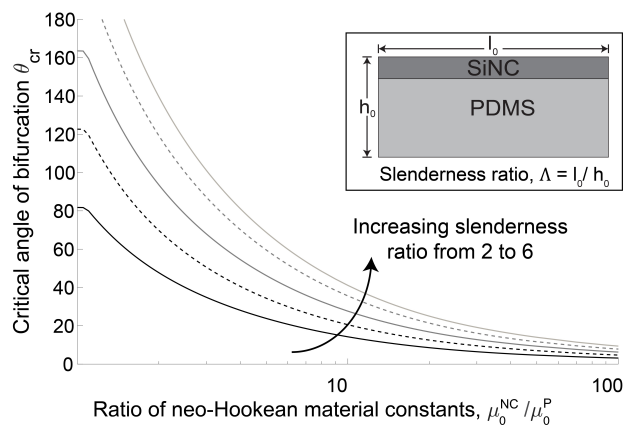


Fig. 6 Critical angles of bifurcation evaluated as a function of ratio of material properties for a PDMS-SiNC bilayer sample. The ratio of the neo-Hookean material parameters is defined as $\bar{\mu}_0 = \mu_0^{NC} / \mu_0^P$. All curves have been calculated for a thickness ratio H included in the range 0.0013–0.0018. Each line represent a different value of slenderness ratio, $\Lambda = 2$, black solid line; $\Lambda = 3$, black dashed line; $\Lambda = 4$, dark gray solid line; $\Lambda = 5$, dark gray dashed line; $\Lambda = 6$, light gray solid line. The insert represents a schematic of the bilayer and defines the slenderness ratio.

3 Results and Discussion

Experimentally, the critical angles of bifurcation were measured for nine samples by performing the finite bending experiment described in Sec. 2.5. The values, reported in Table 1, have been obtained for three experimental groups, characterized by a slenderness ratio $\Lambda = 2, 3$ and 5, each group formed by a total of three samples (see Fig. 6a).

Table 1 Critical angles of bifurcation for different slenderness ratios, expressed in degrees. Angles are reported for $\Lambda = 2, 3$ and 5.

Slenderness ratio, Λ	Critical angle, θ_{cr}	Material parameters ratio, $\bar{\mu}_0$
2	47.33 ± 3.21	1.90 ± 0.13
3	71.33 ± 1.53	1.85 ± 0.05
5	130.67 ± 3.21	1.68 ± 0.04

Employing the model described in Sec. 2.6, we evaluated the critical angle of bifurcation for the bilayered structure, shown in Fig. 6 and Fig. 7. Specifically, after fixing the overall geometry of the sample, namely the thickness ratio H and the slenderness ratio Λ , we calculated the value of the angle representing the onset of bifurcation for each value of the neo-Hookean material parameters ratio, defined as $\bar{\mu}_0 = \mu_0^{NC} / \mu_0^P$. In both Figures, we considered $\bar{\mu}_0$ to be included between 0 and 100, however a pilot study showed that the value of the critical angles plateaus for values of $\bar{\mu}_0$ included between 100 and 10^5 (data not shown). Furthermore, the same pilot study showed that the critical an-

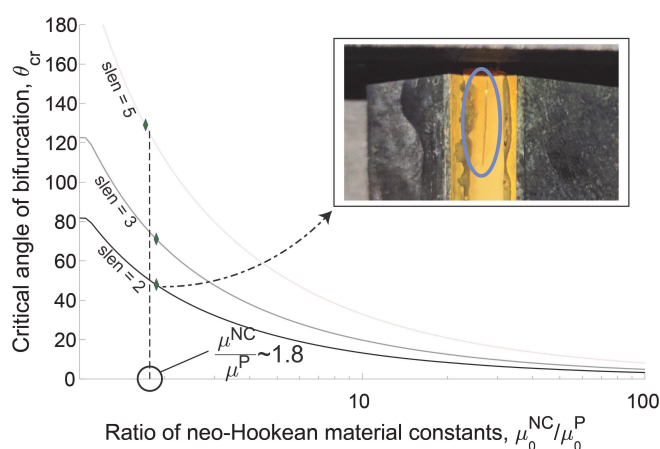


Fig. 7 Plotting points from the experiments on graph obtained by numerical calculations. The ratio of the neo-Hookean material parameters is defined as $\bar{\mu}_0 = \mu_0^{NC} / \mu_0^P$. Shown here are points obtained for $\Lambda = 2, 3$ and 5. Insert shows an instability on the surface of a sample with $\Lambda = 2$.

gle of bifurcation is independent of the thickness ratio H , if H is included in the range 0.0013 – 0.0018. The experimental value measured in this study is included within that range, specifically $H = 0.0017$ on average for the nine samples.

Fig. 6 shows the variation of the critical angle of bifurcation for varying values of the slenderness ratio, specifically for Λ included in the range 2 to 6. For a fixed value of $\bar{\mu}_0$, which is represented by a vertical line in the graph, an increase in the slenderness ratio results in a later appearance of the bifurcation, namely a higher value for the critical angle. This trend is consistent with previously published results^{41,42}.

Fig. 7 shows how we employed the onset of bifurcation to estimate the mechanical properties of the SiNC layer. Briefly, for each value of slenderness ratio considered in the experiments, we calculated the correspondent theoretical sets of bifurcation angles. Then, the critical angle measured experimentally was employed to uniquely identify the corresponding $\bar{\mu}_0$. The experimental value of the critical angle fixed the abscissa of the point in the $\theta_{cr} - \bar{\mu}_0$ plane, represented in Fig. 7. Then, we imposed that the experimental point belonged on the bifurcation threshold curve calculated for the corresponding slenderness ratio, which in turns fixed the ordinate of the point which is $\bar{\mu}_0$. The value estimated for each experimental group, namely for each value of slenderness ratio considered, is reported in Table 1. A vertical dashed line in Fig. 7 represents the average value of $\bar{\mu}_0$ for all the experimental data, which is 1.81 ± 0.12 . We then estimated the value of $\mu_0^P = 190$ kPa by fitting the data collected from the uniaxial tensile test, as described in Sec. 2.4. This gave us a value for the neo-Hookean material coefficient for the SiNC layer of $\mu_0^{NC} 345 \pm 23$ kPa. The neo-Hookean material constant is analogous to the shear modulus for low values of applied strain.

This finding is a clear indicator that the mechanical properties of this materials system are determined by the interactions between SiNCs within the NC layer and between the NC layer and the PDMS. Direct measurements of the mechanical properties of individual silicon nanocrystals via microscope-guided nanoin-

dentation have yielded elastic moduli around 170 GPa,⁵³ several orders of magnitude higher than our measurement of the shear modulus for the SiNC layer on PDMS (assuming incompressible behavior, shear modulus is $\sim 1/3$ of the elastic modulus). Others have produced elastic/Young's modulus estimates for single SiNCs between 70–170 GPa.^{54–56} This range of values (~ 20 –60 GPa for shear modulus) is also consistent with mechanical measurements of thin ribbons of crystalline silicon on PDMS⁵⁷. By contrast, our value of 380 kPa for shear modulus is far lower, and is consistent with the higher porosity of our nanopowder layer as compared to bulk silicon. For example, Gross *et al.* showed that increasing porosity of powder hydroxyapatite coatings leads to decreasing elastic modulus - further, regardless of porosity, the coatings exhibited values of elastic modulus more than 35x smaller than the modulus of single-crystal hydroxyapatite.^{58,59} Similarly, the Young's modulus of aluminum foams is between 10^{-1} and 10^{-3} the value of Young's modulus of solid aluminum, depending on porosity.⁶⁰ Finally, previous results have shown that increased porosity significantly decreases the Young's modulus of polymer thin films deposited on PDMS, when measured by employing mechanical instabilities.⁶¹ The porosity of our layers was difficult to ascertain with high accuracy. However, a preliminary density measurement provided us with a value near the limit for close-packed randomly oriented rigid spheres (volume fraction 0.64). While we did not probe the effects of porosity in this proof-of-concept investigation, the porosity of the SiNC layer is tunable by adjusting reactor properties,^{49,51} and future work will be devoted to determining the relationship between layer porosity and mechanical properties. This versatile method is broadly applicable to extract the mechanical properties of nanoparticle layers on elastomer substrates regardless of material, layer thickness, and density. Our results also offer a unique opportunity in the future to investigate how the NC surface functionality (organic ligand coating, inorganic shell, *etc.*) influences the mechanical behavior of the NC films.

4 Conclusions

In summary, we have used a novel method based on the onset of bifurcation to estimate the mechanical properties of thin layers of nanocrystals on PDMS. In general this method to evaluate mechanical properties of thin films can be extended to any bilayer system of elastomer and nanoparticle thin film, opening up new possibilities for understanding, predicting, and controlling the mechanical behavior of nanoparticle layers in flexible or bendable device technologies, leveraging both the unique optoelectronic properties of nanoparticles together with the mechanical versatility offered by these films.

Additionally, the results obtained from this experiment are exciting because earlier attempts in finding instability formation due to finite bending in a multilayered structure were limited to structures with elastomeric layers only. Here we have reliably shown formation of instabilities in thin SiNC films deposited on PDMS. This invites opportunities to study and develop constitutive models which are better suited to such constituents, in addition to other experimental methods that can perform *in situ* measurements of such a system.

Conflicts of interest

There are no conflicts to declare.

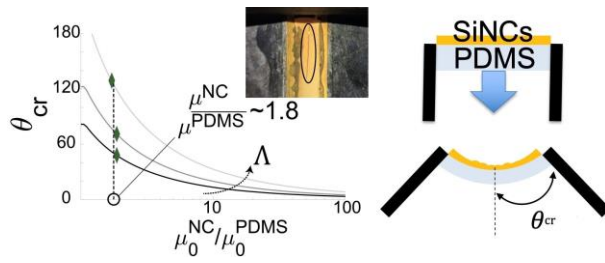
Acknowledgements

This research was supported by the National Science Foundation CMMI Grant #1561964 and College of Engineering, Michigan State University.

Notes and references

- 1 S. Park, G. Wang, B. Cho, Y. Kim, S. Song, Y. Ji, M. H. Yoon and T. Lee, *Nature Nanotechnology*, 2012, **7**, 438–442.
- 2 A. J. Bandodkar, R. Nuñez-Flores, W. Jia and J. Wang, *Advanced Materials*, 2015, **27**, 3060–3065.
- 3 Z. Bao and X. Chen, *Advanced Materials*, 2016, **28**, 4177–4179.
- 4 T. Sekitani, T. Yokota, U. Zschieschang, H. Klauk, S. Bauer, K. Takeuchi, M. Takamiya, T. Sakurai and T. Someya, *Science*, 2009, **326**, 1516–1520.
- 5 T. Takagahara and K. Takeda, *Physical Review B*, 1992, **46**, 15578.
- 6 J. Proot, C. Delerue and G. Allan, *Applied Physics Letters*, 1992, **61**, 1948–1950.
- 7 F. Maier-Flaig, J. Rinck, M. Stephan, T. Bocksrocker, M. Bruns, C. Kubel, A. K. Powell, G. A. Ozin and U. Lemmer, *Nano letters*, 2013, **13**, 475–480.
- 8 S. Fujita and N. Sugiyama, *Applied physics letters*, 1999, **74**, 308–310.
- 9 B. Tian, X. Zheng, T. J. Kempa, Y. Fang, N. Yu, G. Yu, J. Huang and C. M. Lieber, *nature*, 2007, **449**, 885.
- 10 C.-Y. Liu, Z. C. Holman and U. R. Kortshagen, *Nano letters*, 2008, **9**, 449–452.
- 11 M. J. Rose, J. Hajto, P. G. Lecomber, S. M. Gage, W. K. Choi, A. J. Snell and A. E. Owen, *Journal of Non-Crystalline Solids*, 1989, **115**, 168–170.
- 12 R. J. Anthony, D. J. Rowe, M. Stein, J. Yang and U. Kortshagen, *Advanced functional materials*, 2011, **21**, 4042–4046.
- 13 R. J. Anthony, K.-Y. Cheng, Z. C. Holman, R. J. Holmes and U. R. Kortshagen, *Nano letters*, 2012, **12**, 2822–2825.
- 14 A. Van Sickle, J. Miller, C. Moore, R. Anthony, U. Kortshagen and E. Hobbie, *ACS Applied Materials and Interfaces*, 2013, **5**, 4233–4238.
- 15 F. Meinardi, S. Ehrenberg, L. Dharmo, F. Carulli, M. Mauri, F. Bruni, R. Simonutti, U. Kortshagen and S. Brovelli, *Nature Photonics*, 2017, **11**, 177–185.
- 16 C. Wang, D. Hwang, Z. Yu, K. Takei, J. Park, T. Chen, B. Ma and A. Javey, *Nature materials*, 2013, **12**, 899.
- 17 J. R. Greer, W. C. Oliver and W. D. Nix, *Acta Materialia*, 2005, **53**, 1821–1830.
- 18 Y. Yue, P. Liu, Z. Zhang, X. Han and E. Ma, *Nano Letters*, 2011, **11**, 3151–3155.
- 19 X. Han, K. Zheng, Y. Zhang, X. Zhang, Z. Zhang and Z. L. Wang, *Advanced Materials*, 2007, **19**, 2112–2118.
- 20 M. D. Uchic, D. M. Dimiduk, J. N. Florando and W. D. Nix, *Science*, 2004, **305**, 986–989.

- 21 J. Wang, Z. Zeng, C. R. Weinberger, Z. Zhang, T. Zhu and S. X. Mao, *Nature Materials*, 2015, **14**, 594–600.
- 22 L. Wang, J. Teng, X. Sha, J. Zou, Z. Zhang and X. Han, *Nano Letters*, 2017, **17**, 4733–4739.
- 23 L. Wang, P. Guan, J. Teng, P. Liu, D. Chen, W. Xie, D. Kong, S. Zhang, T. Zhu, Z. Zhang, E. Ma, M. Chen and X. Han, *Nature Communications*, 2017, **8**, 1–7.
- 24 Z. Zhang, X. D. Han, Y. F. Zhang, K. Zheng, X. N. Zhang, Y. J. Hao, X. Y. Guo, J. Yuan and Z. L. Wang, *Nano Letters*, 2007, **7**, 452–457.
- 25 L. Wang, X. Han, P. Liu, Y. Yue, Z. Zhang and E. Ma, *Physical Review Letters*, 2010, **105**, 1–4.
- 26 L. Wang, J. Teng, P. Liu, A. Hirata, E. Ma, Z. Zhang, M. Chen and X. Han, *Nature Communications*, 2014, **5**, 1–7.
- 27 J. Y. Chung, A. J. Nolte and C. M. Stafford, *Advanced Materials*, 2011, **23**, 349–368.
- 28 R. Vendamme, T. Ohzono, A. Nakao, M. Shimomura and T. Kunitake, *Langmuir*, 2007, **23**, 2792–2799.
- 29 J. M. Torres, C. M. Stafford and B. D. Vogt, *ACS Nano*, 2009, **3**, 2677–2685.
- 30 C. M. Stafford, B. D. Vogt, C. Harrison, D. Julthongpiput and R. Huang, *Macromolecules*, 2006, **39**, 5095–5099.
- 31 D. Tahk, H. H. Lee and D.-Y. Khang, *Macromolecules*, 2009, **42**, 7079–7083.
- 32 C. Jiang, S. Singamaneni, E. Merrick and V. V. Tsukruk, *Nano Letters*, 2006, **6**, 2254–2259.
- 33 A. J. Nolte, M. F. Rubner and R. E. Cohen, *Macromolecules*, 2005, **38**, 5367–5370.
- 34 C. Lu, I. D'Áunçh, M. Nolte and A. Fery, *Chemistry of Materials*, 2006, **18**, 6204–6210.
- 35 N. Triantafyllidis, *Journal of the Mechanics and Physics of Solids*, 1980, **28**, 221–245.
- 36 G. Dryburgh and R. W. Ogden, *Zeitschrift für Angewandte Mathematik und Physik*, 1999, **50**, 822–838.
- 37 A. N. Gent, *International Journal of Non-Linear Mechanics*, 2005, **40**, 165–175.
- 38 C. D. Coman and M. Destrade, *Quarterly Journal of Mechanics and Applied Mathematics*, 2008, **61**, 395–414.
- 39 A. N. Gent and I. S. Cho, *Rubber Chemistry and Technology*, 1999, **72**, 253–262.
- 40 M. Destrade, M. D. Gilchrist, J. A. Motherway and J. G. Murphy, *Mechanics of Materials*, 2010, **42**, 469–476.
- 41 S. Roccabianca, M. Gei and D. Bigoni, *IMA Journal of Applied Mathematics (Institute of Mathematics and Its Applications)*, 2010, **75**, 525–548.
- 42 S. Roccabianca, D. Bigoni and M. Gei, *Journal of Mechanics of Materials and Structures*, 2011, **6**, 511–527.
- 43 M. Destrade, R. W. Ogden, I. Sgura and L. Vergori, *Proceedings of the Royal Society A*, 2014, **470**, 20130709.
- 44 T. Sigaeva, R. Mangan, L. Vergori, M. Destrade and L. Sudak, *Proceedings of the Royal Society A: Mathematical, Physical and Engineering Sciences*, 2018, **474**, 2212.
- 45 R. Mandal and R. J. Anthony, *ACS applied materials & interfaces*, 2016, **8**, 35479–35484.
- 46 B. N. Jariwala, O. S. Dewey, P. Stradins, C. V. Ciobanu and S. Agarwal, *ACS applied materials & interfaces*, 2011, **3**, 3033–3041.
- 47 L. Mangolini, E. Thimsen and U. Kortshagen, *Nano letters*, 2005, **5**, 655–659.
- 48 D. Jurbergs, E. Rogojina, L. Mangolini and U. Kortshagen, *Applied Physics Letters*, 2006, **88**, 233116.
- 49 Z. C. Holman and U. R. Kortshagen, *Nanotechnology*, 2010, **21**, 335302.
- 50 G. Nava, F. Fumagalli, S. Neutzner and F. Di Fonzo, *Nanotechnology*, 2018, **29**, 465603.
- 51 P. Firth and Z. C. Holman, *ACS Applied Nano Materials*, 2018, **1**, acsanm.8b01334.
- 52 D. Bigoni, *Nonlinear solid mechanics: bifurcation theory and material instability*, Cambridge University Press, 2012.
- 53 W. W. Gerberich, W. M. Mook, C. R. Perrey, C. B. Carter, M. I. Baskes, R. Mukherjee, A. Gidwani, J. Heberlein, P. H. McMurry and S. L. Girshick, *Journal of the Mechanics and Physics of Solids*, 2003, **51**, 979–992.
- 54 H. Sadeghian, C. K. Yang, J. F. L. Goosen, E. Van Der Drift, A. Bossche, P. J. French and F. Van Keulen, *Applied Physics Letters*, 2009, **94**, 1–4.
- 55 W. M. Mook, J. D. Nowak, C. R. Perrey, C. B. Carter, R. Mukherjee, S. L. Girshick, P. H. McMurry and W. W. Gerberich, *Physical Review B - Condensed Matter and Materials Physics*, 2007, **75**, 1–10.
- 56 D. Kilymis, C. Gérard, J. Amodeo, U. Waghmare and L. Pizzagalli, *Acta Materialia*, 2018, **158**, 155–166.
- 57 D. Y. Khang, H. Jiang, Y. Huang and J. A. Rogers, *Science*, 2006, **311**, 208–212.
- 58 K. A. Gross and S. Saber-Samandari, *Surface and Coatings Technology*, 2009, **203**, 2995–2999.
- 59 A. Zamiri and S. De, *Journal of the Mechanical Behavior of Biomedical Materials*, 2011, **4**, 146–152.
- 60 E. Andrews, W. Sanders and L. J. Gibson, *Materials Science and Engineering A*, 1999, **270**, 113–124.
- 61 C. M. Stafford, C. Harrison, K. L. Beers, A. Karim, E. J. Amis, M. R. VanLandingham, H.-C. Kim, W. Volksen, R. D. Miller and E. E. Simonyi, *Nature materials*, 2004, **3**, 545.



The onset of bifurcations during bending is used to estimate the shear modulus of silicon nanocrystal layers on PDMS.